



S-doped α -Fe₂O₃ as a highly active heterogeneous Fenton-like catalyst towards the degradation of acid orange 7 and phenol

Liqin Guo, Feng Chen*, Xiangqun Fan, Wandong Cai, Jinlong Zhang

Key Lab for Advanced Materials and Institute of Fine Chemicals, East China University of Science and Technology, 130 Meilong Road, Shanghai 200237, PR China

ARTICLE INFO

Article history:

Received 16 December 2009

Received in revised form 4 February 2010

Accepted 7 February 2010

Available online 12 February 2010

Keywords:

α -Fe₂O₃/S

Heterogeneous Fenton reaction

Doping

Acid orange 7

Phenol

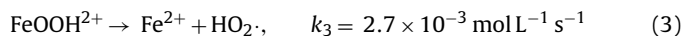
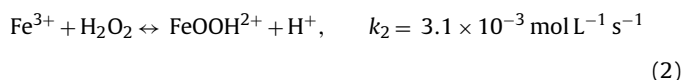
ABSTRACT

S-doped α -Fe₂O₃ (α -Fe₂O₃/S) was synthesized with ferrous sulfate and Na₂S₂O₃ via a hybrid hydrothermal-calcination treatment. The crystal phase, special surface area, morphology of the α -Fe₂O₃/S as well as the chemical state of the sulfur were studied by X-ray diffraction (XRD), scanning electron microscopy (SEM), Raman spectrum and X-ray photoelectron spectroscopy (XPS). The Fenton and photo-Fenton reactivities of the α -Fe₂O₃/S were tested by degrading acid orange 7 (AO7) and phenol. Although α -Fe₂O₃/S showed little Fenton reactivity in the dark, it had an excellent heterogeneous Fenton reaction under either UV or visible irradiation, while other α -Fe₂O₃s were still kept inactive. S element was found to dope into α -Fe₂O₃ in the forms of FeS or FeS₂ in α -Fe₂O₃/S. The doped S element promotes the photo-Fenton reaction of α -Fe₂O₃/S via two roles: retarding the recombination of photogenerated charge carriers and promoting the electron transfer between the peroxide species and iron ions at the interface.

© 2010 Elsevier B.V. All rights reserved.

1. Introduction

Fenton and photo-Fenton processes have been proven to be effective methods to treat organic pollutants in wastewater [1–3]. Their mechanism and kinetics have been widely studied. Hydroxyl radical and superoxide radical were generated in the Fenton reaction, and then effectively degrade and mineralize organics to CO₂, H₂O and some other inorganic substances [4–6].



Although Fenton reagent is regarded as a kind of powerful oxidant, its practical applications in dealing with industry wastewater are facing some disadvantages, e.g. the pH range suitable for reacting is very narrow, and it is costly to remove the iron ions from the system after the reaction was over [7,8].

Many works have been focused on the heterogeneous Fenton process to avoid the disadvantages mentioned above. Various iron-

containing solid compounds were involved in the heterogeneous Fenton reaction in the recent publications. Such iron-containing solid compounds can be (i) iron oxides, such as α -Fe₂O₃ [9], γ -Fe₂O₃ [10], α -FeOOH [9,11], Fe₃O₄ [9], Fe₀/Fe₂O₃ [12] and Fe₀/Fe₃O₄ [13]; (ii) metal elements doped iron oxides, such as vanadium (V) [14], cerium (Ce) [15], niobium (Nb) [16], copper (Cu) [17], manganese (Mn) [18] and doping iron oxides; and (iii) iron oxides containing materials, of which bentonite [19,9], high polymer [20], zeolite [21], mesoporous silica [22,23] and carbon nanotubes [24] are used as carriers.

Among the above heterogeneous Fenton catalysts, α -Fe₂O₃ is the most common crystalline polymorph of Fe₂O₃ and is more chemically and thermally stable than other Fe₂O₃ crystalline polymorphs. Further, α -Fe₂O₃ can be readily prepared by various methods, among which calcination is a most involved method [9,25–29]. However, The Fenton reaction performance of α -Fe₂O₃ is somewhat bad. Comparing with that of γ -Fe₂O₃, γ -FeOOH and α -FeOOH, the reaction activity of the α -Fe₂O₃ is much lower [9,27–29].

Synthetic dyes have been extensively used in textile, paper and printing industries and significant losses are discharged in the effluent during the manufacture and dyeing processes. Many of them are very toxic and carcinogenic, resistant to biological degradation, and their color removal by bioprocessing is difficult and always incomplete. Therefore, decoloration and decomposition of azo-dye using the Fenton reagent had been actively discussed [2,7,9,14]. In this work, a heterogeneous Fenton catalyst, S-doping α -Fe₂O₃ (α -Fe₂O₃/S), was prepared by hydrothermal combining with calcinations method. The Fenton reaction performance of α -Fe₂O₃/S

* Corresponding author. Tel.: +86 21 6425 2062; fax: +86 21 6425 2062.

E-mail addresses: cloud1133@163.com (L. Guo), fengchen@ecust.edu.cn (F. Chen), fxq5566@163.com (X. Fan), caiwangdong1225@163.com (W. Cai), jlzhang@ecust.edu.cn (J. Zhang).

was examined with the degradation of a typical azo-dye, acid orange 7 (AO7). The α -Fe₂O₃/S catalyst exhibited a significantly higher reaction activity than normal α -Fe₂O₃ materials.

2. Experimental

2.1. Reagents and materials

FeSO₄·7H₂O, Na₂S₂O₃ and Fe₂O₃ were of AR and purchased from Sinopharm Chemical Reagent. NaOH, H₂SO₄, H₂O₂, and NH₃·H₂O were obtained from Lingfeng Chemical Reagent. AO7 (Scheme 1, λ_{\max} = 483 nm) was obtained from Acros and used without further purification. Doubly distilled water was used throughout the work.

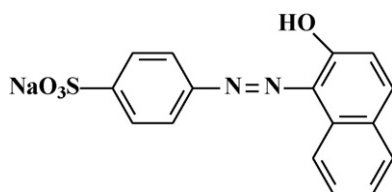
2.2. Preparation of catalysts

The heterogeneous Fenton catalyst was prepared as follows. Ferrous ion solution was obtained by dissolving 5.08 g (0.018 mol) FeSO₄·7H₂O and 2.48 g (0.01 mol) Na₂S₂O₃ in 30 mL water. A solution of 1.0 mol/L NaOH (20 mL) was then added dropwise into the as-prepared solution. The obtained black suspension was kept stirring for 30 min and then hydrothermally treated at 150 °C for 24 h. The suspension (dark gray green) was filtered, washed repeatedly by water and absolute ethanol, dried in a vacuum at 60 °C and calcined at 500 °C for 4 h. The final obtained powder was labeled as α -Fe₂O₃/S for further use.

Besides the commercial α -Fe₂O₃, Fe₂O₃ catalysts were also synthesized with other two procedures for comparing. With the above procedure, Fe₂O₃-I was prepared by using FeCl₂·4H₂O (0.018 mol) instead of FeSO₄·7H₂O and Na₂S₂O₃. Fe₂O₃-II was prepared according to Ref. [26]. An aqueous solution (70 mL) contained 1.23 g CH₃COONa and 1.35 g FeCl₃·6H₂O was hydrothermal treated in a 100 mL Teflon-lined stainless autoclave, keeping 100 °C for 12 h. A brown precipitation obtained was filtered, washed and then calcined at 550 °C for 6 h to get Fe₂O₃-II.

2.3. Catalyst characterization

X-ray diffraction (XRD) measurement was carried out by using a Rigaku D/MAX 2550 VB/PC X-ray diffractometer (Cu K α radiation, λ = 0.154056 nm). Scanning electron microscopy (SEM) was conducted using from JSM-6360 LV, (JEOL). The surface of the samples was analyzed with micro Raman spectroscopy (Renishaw inVia + Reflex spectrometer). Raman spectra were recorded at room temperature employing He–Ne laser (λ = 632.8 nm) with a laser power of 9 mW. X-ray photoelectron spectroscopy (XPS, Perkin-Elmer PHI 5000C ESCA system) with Al K α radiation was operated at 250 W. Binding energies were calibrated versus the carbon signal at 284.60 eV. The BET specific surface areas (S_{BET}) of the samples were determined by using nitrogen adsorption in a Micromeritics ASAP 2010 nitrogen-adsorption apparatus. All the samples were degassed at 473 K prior to the measurement. The content of S element was detected through inductive coupled plasma emission spectrometer (ICP-AES, IRIS 1000, Thermo Elemental) after the α -Fe₂O₃/S was entirely dissolved by HCl (37%).



Scheme 1. Chemical structure of AO7.

2.4. Heterogeneous Fenton reaction performance measurement

All experiments were conducted in a cylindrical quartz tube under magnetic stirring. UV irradiation was carried out directly using a 300 W high-pressure Hg lamp, which was surrounded by a quartz jacket to allow for water-cooling. Visible irradiation was carried out using a 1000 W halogen lamp. The short wavelength components (λ < 420 nm) of the visible light were cut off using a glass optical filter (JB420). In a typical procedure, desired concentrations of AO7 (100 mL, 35 mg/L) or phenol (40 mg/L) and catalyst powder (0.10 g/L) were firstly mixed under stirring for 30 min in dark (25 °C water bath). Then H₂O₂ was added into the solution. The reaction was timed as soon as the H₂O₂ was added. At given reaction time intervals, 3.0 mL samples were taken out, and immediately immitted into 1.0 mL phosphate buffer solution to avoid further reaction (total phosphate concentration of 0.20 mol L⁻¹, pH 8.0) and then filtered. The residual concentration of AO7 was then determined by measuring its absorbance at 484 nm on a UV/vis spectrophotometer (Unico, 4802).

2.5. Leached iron ion detection

Leached iron ion in the aqueous solution after Fenton reaction was measured using 1,10-phenanthroline as a complexing agent. Reaction solution of 4 mL was sampled, mixed with 2 mL 1,10-phenanthroline solution (1.0 g/L), and centrifuged immediately. The as-obtained supernatant was placed still for 20 min. Then the absorbance of ferrous phenanthroline at 510 nm was measured and used to calculate the concentration of leached iron in the solution.

3. Results and discussion

3.1. Structure characterization of catalyst

Fig. 1 presents the XRD patterns of various iron oxides and the intermediate precipitations during the preparation of α -Fe₂O₃/S catalyst. The black powder directly produced by the reaction of FeSO₄ and Na₂S₂O₃ under alkali condition was a mixture (Fig. 1(a)) that consists of several species such as FeO(OH), Fe₃O₄, FeS and Fe₁₂S₁₁O₅₁. They were generated via the reactions of ferrous ions with S₂O₃²⁻ and oxygen in alkali condition. The black powder was oxidized partly by the dissolved O₂ in the solution during the hydrothermal treatment, thus, α -Fe₂O₃ phase emerged as the main component in the precipitation after hydrothermal treatment (Fig. 1(b)). After calcined in air at 500 °C for 4 h, a typical XRD pat-

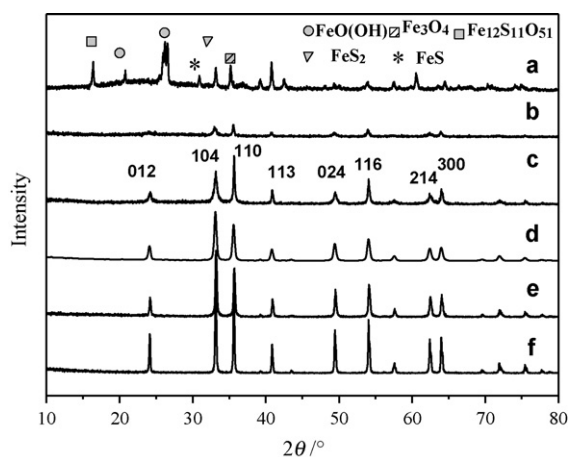


Fig. 1. XRD patterns of (a) black powder produced by the reaction of FeSO₄ and Na₂S₂O₃ in alkali solution, (b) above precipitation after hydrothermal treated, (c) α -Fe₂O₃/S, (d) Fe₂O₃-I, (e) Fe₂O₃-II, and (f) commercial α -Fe₂O₃.

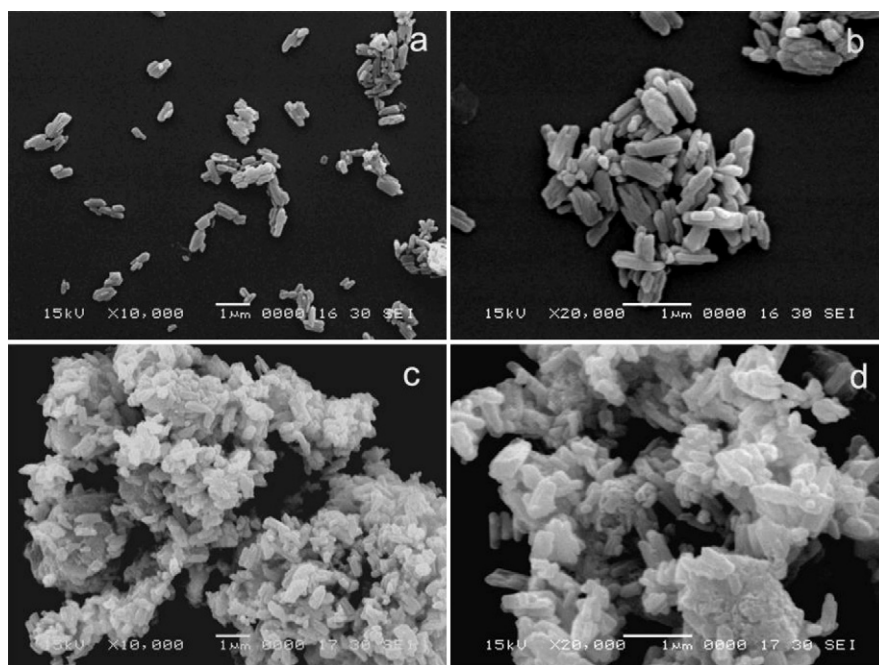


Fig. 2. SEM images of (a) and (b) α -Fe₂O₃/S after hydrothermal treatment but before calcination and (c) and (d) α -Fe₂O₃/S after calcination.

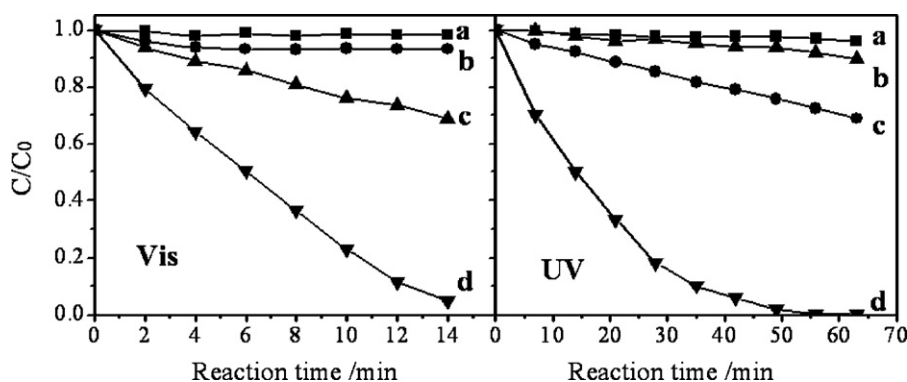


Fig. 3. Degradation of AO7 under UV and visible irradiation. (a) AO7 with H₂O₂ and α -Fe₂O₃/S in the dark, (b) AO7 with H₂O₂ under irradiation, (c) AO7 with α -Fe₂O₃/S under irradiation, (d) AO7 with H₂O₂ and α -Fe₂O₃/S under irradiation. α -Fe₂O₃/S: 10 mg, [H₂O₂], 1.94 mmol/L; pH, 6.85.

tern of α -Fe₂O₃ (Fig. 1(c), JCPDS-33-0664) was clearly observed, which means a formation of perfect α -Fe₂O₃ nanocrystallite after calcinations for α -Fe₂O₃/S. The XRD patterns of three other iron oxides, commercial α -Fe₂O₃, Fe₂O₃-I and Fe₂O₃-II were also fitted well with that of α -Fe₂O₃. Thus, iron oxides involved in this work are all α -Fe₂O₃.

Fig. 2 presents the SEM images of the gray green precipitation after hydrothermal treatment and the final α -Fe₂O₃/S catalyst. The precipitation before calcination has a short-rod-like form with a length of 500–800 nm and a diameter of ca. 200 nm. Morphologies of the finally obtained α -Fe₂O₃/S are also short-rod-like and almost have no change on the configuration. However, it shows a tendency of aggregation comparing with the precipitation before calcination.

3.2. Photo-Fenton reaction performance of α -Fe₂O₃/S catalyst

The photo-Fenton reaction performance of α -Fe₂O₃/S catalyst was observed with the degradation of AO7 dye and phenol (Figs. 3 and 4). AO7 is an azo-dye and relatively photo-stable; AO7 homogeneous solution irradiated with UV or visible light showed no change in whole reaction time range (data not shown). UV

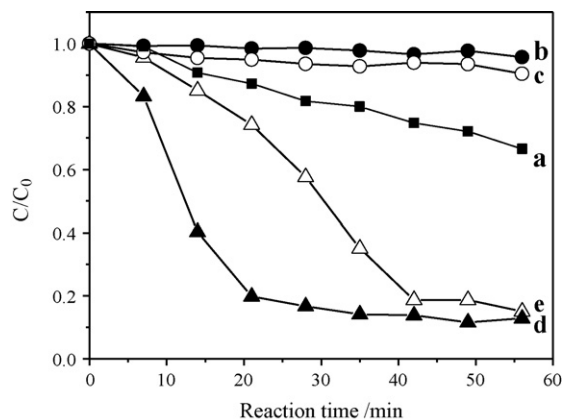


Fig. 4. Fenton degradation of 40 mg/L phenol under UV and visible irradiation. (a) α -Fe₂O₃/S and H₂O₂ in the dark, (b) α -Fe₂O₃/S under UV irradiation, (c) α -Fe₂O₃/S under visible irradiation, (d) α -Fe₂O₃/S and H₂O₂ under UV irradiation, and (e) α -Fe₂O₃/S and H₂O₂ under visible irradiation.

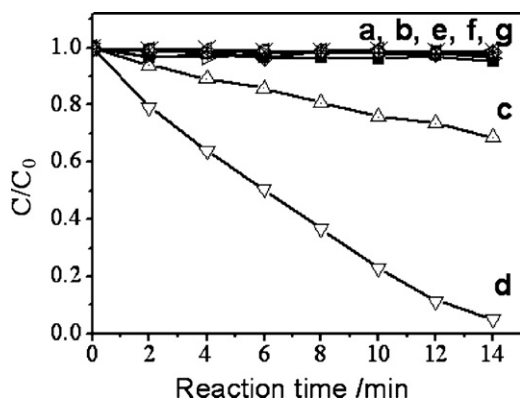


Fig. 5. Photo-Fenton degradation of AO7 under visible light irradiation. (a) AO7 only, (b) AO7 with H₂O₂, (c) AO7 with α-Fe₂O₃/S, (d) AO7 with H₂O₂ and α-Fe₂O₃/S, (e) AO7 with H₂O₂ and commercial α-Fe₂O₃, (f) AO7 with H₂O₂ and Fe₂O₃-I, and (g) AO7 with H₂O₂ and Fe₂O₃-II. [H₂O₂], 1.94 mmol/L; pH, 6.85.

photo-Fenton reaction presented an entirely degradation of AO7 with α-Fe₂O₃/S in 63 min, while only 10.4% of AO7 loss occurred by the reaction of AO7 and H₂O₂ under UV irradiation. AO7 loss of ca. 31% with α-Fe₂O₃/S under UV irradiation in 63 min should be due to the photocatalysis of α-Fe₂O₃ [30].

Under the visible irradiation, AO7 was hardly degraded in the only presence of H₂O₂. As we know, H₂O₂ cannot be excited with visible photon. α-Fe₂O₃/S combined with visible irradiation smoothly degraded the AO7, which should be due to the photocatalysis (and dye-sensitized photocatalysis) of α-Fe₂O₃/S. α-Fe₂O₃ with a band gap of 2.2 eV can be excited by the photons with wavelength shorter than 530 nm to generate CB electrons and VB holes. The degradation of AO7 was greatly enhanced in the presence of H₂O₂ and α-Fe₂O₃/S under visible irradiation ca. 95% of the AO7 was degraded in 14 min (Fig. 3). The electron transfer from the excited dye to α-Fe₂O₃ reduced Fe³⁺ to Fe²⁺, which significantly promoted the reaction, i.e. a dye-sensitized visible light photo-Fenton reaction was carried out.

Fig. 4 shows the degradation of phenol with of α-Fe₂O₃/S under various conditions. α-Fe₂O₃/S with visible irradiation only degraded phenol ca. 5% in 1 h, which suggested that the obvious degradation of AO7 under the similar condition (Fig. 3(c)) was mainly because of the dye-sensitized photocatalysis. α-Fe₂O₃/S with H₂O₂ degraded phenol smoothly in the dark, which process was then greatly enhanced with either UV or visible irradiation. Surely, α-Fe₂O₃/S acted as a very excellent heterogeneous photo-Fenton catalyst here.

Most works show that α-Fe₂O₃ is not so active as other iron oxides in heterogeneous Fenton reaction, e.g. reaction constant for α-Fe₂O₃ was only ca. 1.5% of that for Fe₃O₄ with H₂O₂ in heterogeneous Fenton reaction [29], and smaller than that of amorphous FeOOH [9]. Matta et al. [27] even suggested that α-Fe₂O₃ is inactive compared with other iron oxides in Fenton degradation of 2,4,6-trinitrotoluene. In a word, α-Fe₂O₃ is not a preferable catalyst in general. The visible light-induced photo-Fenton degradations of AO7 with various α-Fe₂O₃ materials were studied in Fig. 5. None of the α-Fe₂O₃ materials except α-Fe₂O₃/S exhibited a significant photo-Fenton reaction activity.

The special surface area of α-Fe₂O₃/S, commercial α-Fe₂O₃, Fe₂O₃-I, and Fe₂O₃-II is 27.52 m²/g, 3.39 m²/g, 14.48 m²/g, and 22.70 m²/g, respectively. α-Fe₂O₃/S catalyst had a similar surface area as the others. Therefore, the reaction activity difference among the various α-Fe₂O₃ catalysts is not likely because of their differences in surface area. Among the three reference α-Fe₂O₃ involved in Fig. 5, Fe₂O₃-I was prepared in the same procedure of α-Fe₂O₃/S except FeSO₄ and Na₂S₂O₃ were replaced by FeCl₂. Thus, the partic-

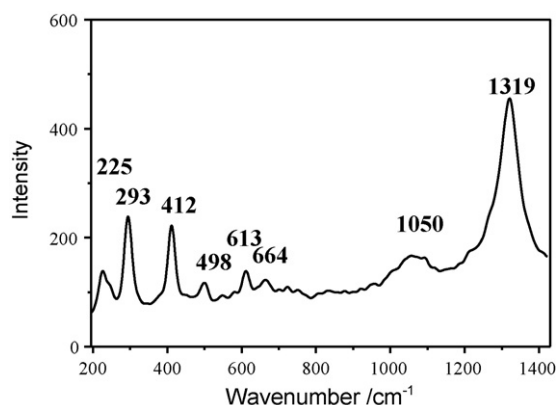


Fig. 6. Raman spectrum of the α-Fe₂O₃/S sample.

ipation of sulfur element must be responsible to the Fenton reaction activity enhancement of α-Fe₂O₃/S here.

After 30 min of reaction for the degradation of AO7, the leached irons from α-Fe₂O₃/S had concentrations of 15 × 10⁻⁶ mol/L (UV experiment) and 18 × 10⁻⁶ mol/L (vis experiment), which correspond to 0.12% and 0.14% of the catalyst mass, respectively. The leached irons may contribute to the overall catalytic activity. However, considering that the leached iron in the neutral solution should be complexed with organics, which significantly reduces the Fenton reactivity of the leached iron. The contribution of leached iron ion to the overall catalytic activity is limited.

3.3. The chemical state of different elements in α-Fe₂O₃/S catalyst

The amount of S in α-Fe₂O₃/S catalyst was 5.62 wt.% from the ICP data. The chemical states of different elements in α-Fe₂O₃/S catalyst were further analyzed with Raman and XPS spectroscopy as shown in Figs. 6 and 7. Raman spectrum peaks of the positions at 225 cm⁻¹, 293 cm⁻¹, 412 cm⁻¹, 498 cm⁻¹, 613 cm⁻¹ and 1319 cm⁻¹ are the characteristic Raman peaks of α-Fe₂O₃. It was frequently reported that α-Fe₂O₃ has characteristic Raman peaks at 225 cm⁻¹, 293 cm⁻¹, 411 cm⁻¹, 498 cm⁻¹, 612 cm⁻¹ and 1320 cm⁻¹ [31]. Signal at 664 cm⁻¹ was also mentioned in the literatures several times in the Raman characterization of α-Fe₂O₃ nanosystem [32–34]. It was suggested that surface disorder of α-Fe₂O₃ nanoparticles sometimes induces the breaking of symmetry properties for scattering the longitudinal optical (LO) phonon, thus, a Raman-forbidden LO Eu mode is activated and appears in Raman spectrum as an extrinsic signal [32]. FeS was reported [35,36] to present characteristic Raman peak at 282 cm⁻¹, which is not observed. Although this peak is possibly covered by the Raman signals of α-Fe₂O₃ as it is very close to the α-Fe₂O₃ signal at 293 cm⁻¹, FeS, if existed, should be limited in a very low level. Typical signal for FeS₂ at 344 nm is also not presented in the Raman spectrum. Free SO₄²⁻ (HSO₄⁻) species [38] has characteristic peaks at 425 cm⁻¹, 590 cm⁻¹, 900 cm⁻¹, 980 cm⁻¹, 1050 cm⁻¹, 1090 cm⁻¹ and 1200 cm⁻¹. However, the location of these peaks is readily to be altered with strong interactions between the SO₄²⁻ and iron ions (or iron oxide); e.g. peaks for SO₄²⁻ in Fe₂(SO₄)₃ were reported at 1010 cm⁻¹, 1028 cm⁻¹, and 1047 cm⁻¹ [37]. In this work, a broad peak around 1050 cm⁻¹ (and a shoulder around 1200 cm⁻¹) should be due to the surface adsorbed SO₄²⁻.

Fig. 7 shows the fine XPS spectra of Fe2p3/2, O1s and S2p of α-Fe₂O₃/S before and after calcination. The BE of O1s for lattice oxygen of α-Fe₂O₃ is around 529.8 eV as reported [39], while the BE of O1s for -OH species in α-FeOOH or chemical bonded -OH group on the surface of α-Fe₂O₃ is 531.9 eV or 532.0 eV [39]. As for O1s in SO₄²⁻, the BE should be around 533 eV [40]. Before the 500 °C

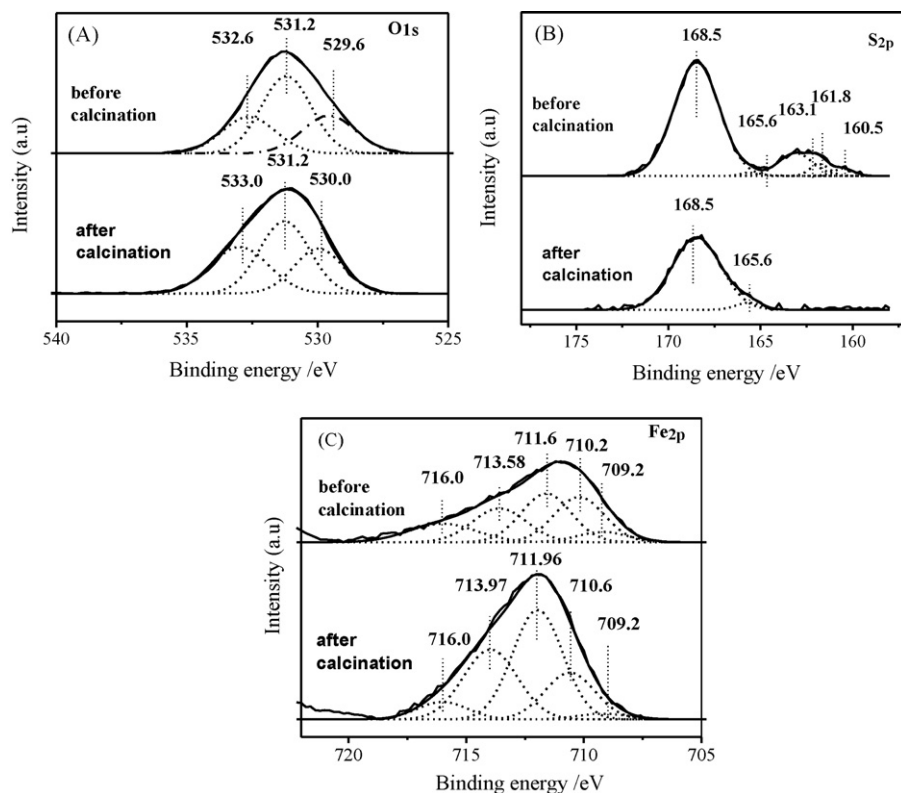


Fig. 7. The fine XPS spectra of (a) O1s, (b) S2p and (c) Fe2p3/2 of α -Fe₂O₃/S before and after 500 °C calcinations.

calcination, the binding energy of O1s photoelectrons exhibited a broad peak around 531.2 eV, which can be fitted into three contributions: 529.6 eV, 531.2 eV and 532.6 eV. In addition to the peak originating from the α -Fe₂O₃ lattice oxygen (529.6 eV), the peak at 531.2 eV can be attributed to the oxygen of the –OH group at the surface of α -Fe₂O₃ [39], while that at 532.6 eV should be from the oxygen in SO₄^{2–} [40]. After the 500 °C calcination, BE of O1s was also fitted with three contributions; however, the peaks had a blue shift of ca. 0.4 eV than those before the calcinations, as well as the ratio of oxygen attributed to SO₄^{2–} increased from 24.9% to 31.6% among the three oxygen species. It seems that the SO₄^{2–} species build a more oxidizing environment in the α -Fe₂O₃.

Iron sulfide and its oxidized products were widely studied with XPS spectra [40–44]. The BEs of S2p photoelectrons were reported distributing from 160 eV to 169 eV, among which the BEs of ferrous bonded S_n^{2–}, S₂^{2–} and S^{2–}, SO₃^{2–}, SO₄^{2–} are around 163.5 eV, 162.2 eV, 161.0 eV, 166.7 eV, and 168.0 eV [40–42]. Fig. 7(b) shows the fine XPS spectra of S2p of α -Fe₂O₃/S. The XPS spectrum of S2p before the calcination has two broad peaks around 163.0 eV and 168.5 eV, which can be fitted into five contributions. The main fitting peak at 168.5 eV should be contributed to SO₄^{2–}, while contributions located at 163.1 eV, 161.8 eV, and 160.5 eV proved the existence of S_n^{2–}, S₂^{2–} and S^{2–}. The small contribution at 165.6 eV, which can also be observed for α -Fe₂O₃/S after calcinations, should be from the ferric ion bonded S (Fe^{III}–S) [44], i.e. from the sulfide that replaces the oxygen in the α -Fe₂O₃ lattice.

During the calcination, reduced forms of S element (S_n^{2–}, S₂^{2–} and S^{2–}) were oxidized to high-valence S (SO₄^{2–}, SO₂); meanwhile, some of the sulfur species was volatilized to the atmosphere, which can be partly reflected by the S amount decrease in the α -Fe₂O₃/S after calcinations—the ratio of S decreased from 12.3 at.% to 5.3 at.% calculated from the survey XPS spectra data. ICP measurement also showed the content of S in the α -Fe₂O₃/S was ca. 4.5 at.%, a little bit lower than that calculated from XPS. It is most probably

because the S element distribution was not uniform and the local S concentration was relative higher on the surface of the α -Fe₂O₃/S. The BE peak of S2p photoelectrons can be fitted into two peaks, one for SO₄^{2–} and another for Fe^{III}–S. Surely, the ratio of Fe^{III}–S was obviously increased after calcinations, which means that some of the S element was dispersed into the lattice of α -Fe₂O₃ and replaced the lattice oxygen to form Fe^{III}–S. The possible reasons that Raman signals of sulfide were not observed in Fig. 6 should be due to (1) the small concentration (0.25%) of sulfide involved and (2) the signals of sulfide may be covered by that of α -Fe₂O₃.

After the hydrothermal treatment under the 150 °C, most of the iron ion was oxidized to ferric ion, whose chemical states are investigated in Fig. 7. Fig. 7(c) shows the fine XPS spectra of Fe2p3/2 of α -Fe₂O₃/S. Fe species of α -Fe₂O₃/S presents a broad BE peak around 711 eV. Before the calcination, the BE of Fe2p3/2 photoelectrons can be fitted into five contributions at 709.2 eV, 710.2 eV, 711.6 eV, 713.6 eV and 716.0 eV. The major contribution located at 711.6 eV is assigned to the lattice Fe^{III} in α -Fe₂O₃, which makes up 29.3% of total Fe species. According to the previous reported literatures [41,43], the weak contribution at 709.2 eV belongs to the sulfide bonded iron (Fe^{III}–S and/or Fe^{II}–S), while contributions of binding energy at 710.2 and 713.6 eV are assigned to (O) Fe–OH and Fe^{III}–SO₄^{2–} [42], respectively. The contribution at 716.0 eV with a FWHM of 3.4 eV ascribes to the surface iron species and the satellite signal of ferrous species. It has been confirmed that a decrease in the coordination numbers of ferric cations located at the surface provides some effect on the BE [44]; thus, shifts the BE value of Fe^{III} from 711.6 eV to 716.0 eV. On the other hand, ferrous species was reported to have a satellite BE peak around 716–718 eV [43]. Since the content of ferrous ion was relatively low after hydrothermal treatment, and the BEs of ferrous ions are always close to those of ferric ions [43], the BE contributions from ferrous ions were not distinctly separated from those of ferric ions. However, some definite changes can be observed between the fine XPS spectra of Fe2p3/2

Table 1Chemical states of Fe, O and S elements and their corresponding BEs in α -Fe₂O₃/S.

Regions	Species	BE (eV) [FWHM] of α -Fe ₂ O ₃ /S			
		Before calcination	Area (%)	After calcination	Area (%)
Fe2p	Surface Fe ^{III} species and satellite of Fe ^{II}	716.0 [3.4]	15.2	716.0 [2.5]	6.8
	Fe ₂ (SO ₄) ₃	713.6 [2.7]	22.1	714.0 [2.7]	29.6
	α -Fe ₂ O ₃	711.6 [2.5]	29.3	712.0 [2.5]	43.0
	Fe–OH	710.2 [2.5]	27.3	710.6 [2.5]	18.3
	Fe ^{III} –S/Fe ^{II} –S/Fe ^{II} –S _n	709.2 [2.5]	6.2	709.2 [2.5]	2.2
O1s	SO ₄ ^{2–}	532.6 [2.4]	24.9	533.0 [2.6]	31.6
	Fe ^{III} –OH/FeOOH	531.2 [2.3]	49.4	531.2 [2.3]	42.6
	α -Fe ₂ O ₃	529.6 [2.4]	25.7	530.0 [2.2]	25.8
S2p	SO ₄ ^{2–}	168.5 [2.9]	81.2	168.5 [3.1]	95.3
	Fe–S	165.6 [1.0]	0.8	165.6 [1.6]	4.7
	S _n ^{2–}	163.1 [2.2]	12.1		
	S ₂ ^{2–}	161.8 [1.2]	3.5		
	S ^{2–}	160.5 [1.3]	2.3		

before and after calcinations. Although it can also be fitted with five contributions for the BE of Fe2p3/2 photoelectrons after calcination, there is a blue shift for those contributions, which means a relative electron-lack environment. Further, the FWHM (2.5 eV) and the intensity of the contribution at 716.0 greatly decrease. Since the ferrous ions should be oxidized during the calcination, the obvious width narrowing of the contribution at 716.0 eV should be most probably because of the disappearance of the satellite BE signal of ferrous ion. The contribution at 709.2 eV decreased significantly, which means the amount of the iron species that bonded with the sulfur (Fe^{III}–S and/or Fe^{II}–S) was lowered after calcination, which is consistent with the results observed in the fine XPS spectra of S2p photoelectrons. In addition, the amount of OFe(OH) decreased while amounts of α -Fe₂O₃ and Fe₂(SO₄)₃ increased after calcination.

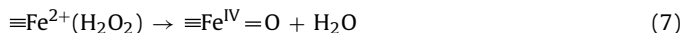
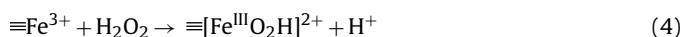
The BE values of the O1s, S2p and Fe2p are summarized in Table 1, which also presented the detailed FWHM and area percentage for every species. Surely, the as-prepared α -Fe₂O₃/S catalyst is an S-doped α -Fe₂O₃ nanocrystal, with a great amount of surface-bonded sulfate group.

3.4. Proposed photo-Fenton reaction mechanism for α -Fe₂O₃/S

Compared with normal α -Fe₂O₃, both the Fenton and photo-Fenton reaction reactivity of the α -Fe₂O₃/S are greatly enhanced. Since the XPS data disagree the existence of Fe²⁺, the main difference occurs on the α -Fe₂O₃/S should ascribe to sulfur species. There are two kinds of sulfur species existing in the α -Fe₂O₃/S: surface adsorbed sulfate and lattice doped sulfide.

In order to reveal the intrinsic factor for the reactivity improvement of α -Fe₂O₃/S, some controlled experiments were carried out and as shown in Fig. 8. Soaking the α -Fe₂O₃/S in H₂O₂ aqueous solution for 15 min did not alter its photo-Fenton reactivity, which suggested again that iron ion component in catalyst was in ferric form but not ferrous form. Fe₂O₃-II was stirred in 0.42 M Na₂SO₄ aqueous solution (pH 4.0) for 48 h, and the calcined to obtain sulfated Fe₂O₃-II. Alternatively, 0.1 g/L of SO₄^{2–} was added directly into the AO7 solution with Fe₂O₃-II. Therefore, adsorption equilibrium of SO₄^{2–} would be built on the surface of Fe₂O₃-II with either modification. Both modifications, however, showed little effect on the photo-Fenton reactivity of Fe₂O₃-II. Thus, it seems that the reactivity improvement of α -Fe₂O₃/S is due to the sulfide-doping.

The doped S element promotes the photo-Fenton reaction of α -Fe₂O₃/S via two roles. The first, the S-doping, most probably, changed the interfacial reaction process of iron ions with H₂O₂ (Eqs. (4)–(7)) [45,46].



Either commercial α -Fe₂O₃ or α -Fe₂O₃-I and α -Fe₂O₃-II hardly had any heterogeneous Fenton-like reactivity; however, α -Fe₂O₃/S degraded AO7 and phenol some in the dark with H₂O₂ (Fig. 4(a))—although slightly. It means that the heterogeneous Fenton-like reactivity of α -Fe₂O₃/S was enhanced by S doping. The hybrid molecular orbitals of sulfide bonded iron ion surely have more extended space than that of oxygen bonded iron ions, which results in more orbital-overlapping and favors the orbital-interaction between the iron ions and surface peroxide species as indicated by selection rule. Thus, the electron transfer between the peroxide species and iron ions (Eqs. (5) and (7)) is enhanced; and consequently, induces higher Fenton reactivity for AO7 and phenol degradations.

Second, the doped S element forms a new trap-state inside the band gap of α -Fe₂O₃, which is very similar as that of S doped TiO₂ [47–50]. α -Fe₂O₃ irradiated with UV or visible light induces photocatalytic processes [8,45,46,51], which are shown as follows:

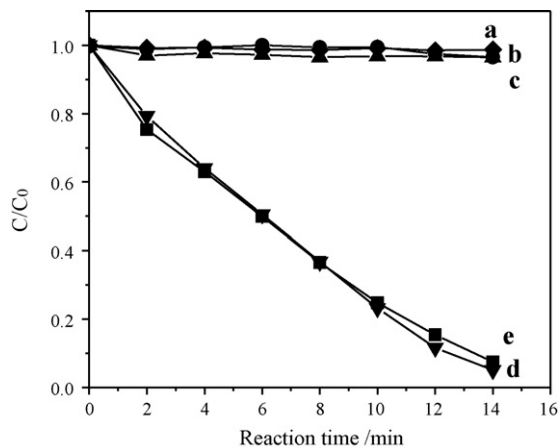
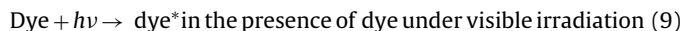
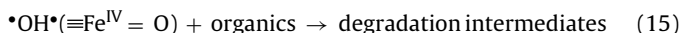
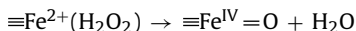
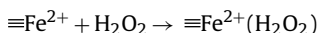
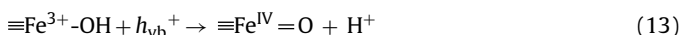


Fig. 8. Photo-Fenton degradation of AO7 under visible irradiation with various catalysts. (a) Fe₂O₃-II, (b) sulfated Fe₂O₃-II, (c) Fe₂O₃-II in the presence of SO₄^{2–} ([SO₄^{2–}] 0.1 g/L), (d) α -Fe₂O₃/S, and (e) H₂O₂-soaked α -Fe₂O₃/S.



The charge carrier recombination (Eq. (11)) in the $\alpha\text{-Fe}_2\text{O}_3$ is quite fast. The electron-hole recombination mediated by intrinsic mid-band gap states and trap-states in the $\alpha\text{-Fe}_2\text{O}_3$ was reported to have a half-life time less than 8 ps [52]. Therefore, the photocatalytic reactivity of $\alpha\text{-Fe}_2\text{O}_3$ was greatly limited. The trap-state from the doped S element, which acts as a defect state, tends to trap the charge carriers as soon as they were generated, and thus, retards their recombination (Eq. (11)). Thus, the degradation rate of AO7 (and phenol) with $\alpha\text{-Fe}_2\text{O}_3/\text{S}$ (Eq. (15)) was much faster than that with all other kinds of $\alpha\text{-Fe}_2\text{O}_3$, either in the presence of H_2O_2 or in the absence of H_2O_2 , as more ferryl species and hydroxyl radical can be produced (Eqs. (13), (14), (6), and (7)).

4. Conclusions

S-doped $\alpha\text{-Fe}_2\text{O}_3$ ($\alpha\text{-Fe}_2\text{O}_3/\text{S}$) was synthesized with ferrous sulfate and $\text{Na}_2\text{S}_2\text{O}_3$ via a hybrid hydrothermal-calcination treatment. Although $\alpha\text{-Fe}_2\text{O}_3/\text{S}$ showed little Fenton reactivity in the dark, it had an excellent heterogeneous Fenton reaction under either UV or visible irradiation, while other $\alpha\text{-Fe}_2\text{O}_3$ s were still un-activated. S element was found to be doped into $\alpha\text{-Fe}_2\text{O}_3$ in the forms of FeS or FeS_2 in $\alpha\text{-Fe}_2\text{O}_3/\text{S}$. The doped S element promotes the photo-Fenton reaction of $\alpha\text{-Fe}_2\text{O}_3/\text{S}$ via two roles: retarding the recombination of photogenerated charge carriers and promoting the electron transfer between the peroxide species and iron ions at the interface.

Acknowledgment

This work was supported by the National Science Foundation of China (20777015).

References

- [1] C. Duesterberg, W.J. Cooper, T.D. Waite, *Environ. Sci. Technol.* 39 (2005) 5052–5058.
- [2] J.M. Monteagudo, A. Durán, C. López-Almodovar, *Appl. Catal. B: Environ.* 83 (2008) 46–55.
- [3] A. Zapata, T. Velegraki, J.A. Sánchez-Pérez, D. Mantzavinos, M.I. Maldonado, S. Malato, *Appl. Catal. B: Environ.* 88 (2009) 448–454.
- [4] C. Walling, *Acc. Chem. Res.* 8 (1975) 125–131.
- [5] C. Walling, A. Goosen, *J. Am. Chem. Soc.* 95 (1973) 2987–2991.
- [6] N. Masomboon, C. Ratanatamskul, M.C. Lu, *Environ. Sci. Technol.* 43 (2009) 8629–8634.

- [7] M.L. Luo, D. Bowden, P. Brimblecombe, *Appl. Catal. B: Environ.* 85 (2009) 201–206.
- [8] M.I. Pariente, F. Martínez, J.A. Melero, J.Á. Botas, T. Velegraki, N.P. Xekoukoulotakis, D. Mantzavinos, *Appl. Catal. B: Environ.* 85 (2008) 24–32.
- [9] J. Feng, X. Hu, P.L. Yue, *Environ. Sci. Technol.* 38 (2004) 5773–5778.
- [10] Q. Lan, F.B. Li, C.S. Liu, X.Z. Li, *Environ. Sci. Technol.* 42 (2008) 7918–7923.
- [11] I.R. Guimaraes, L.C.A. Oliveira, P.F. Queiroz, T.C. Ramalho, M. Pereira, D. Fabris, J.D. Ardisson, *Appl. Catal. A: Gen.* 347 (2008) 89–93.
- [12] Y. Nie, C. Hu, L. Zhou, J. Qu, *Appl. Catal. B: Environ.* 82 (2008) 151–156.
- [13] R.C.C. Costa, F.C.C. Moura, J.D. Ardisson, *Appl. Catal. B: Environ.* 83 (2008) 131–139.
- [14] J. Deng, J. Jiang, Y. Zhang, X. Lin, C. Du, Y. Xiong, *Appl. Catal. B: Environ.* 84 (2008) 468–473.
- [15] E. Heckert, S. Seal, W. Self, *Environ. Sci. Technol.* 42 (2008) 5014–5019.
- [16] L.C.A. Oliveira, M. Goncalves, M.C. Guerreiro, *Appl. Catal. A: Gen.* 316 (2007) 117–124.
- [17] I.R. Guimaraes, A. Giroto, L.C.A. Oliveira, M.C. Guerreiro, D.Q. Lima, J.D. Fabris, *Appl. Catal. B: Environ.* 91 (2009) 581–586.
- [18] Y.F. Han, F. Chen, Z. Zhong, K. Ramesh, L. Chen, D. Jian, W.W. Ling, *J. Chem. Eng.* 134 (2007) 276–281.
- [19] J. Feng, X. Hu, P.L. Yue, *Environ. Sci. Technol.* 38 (2004) 269–275.
- [20] S. Wei, Y. Zhu, Y. Zhang, J. Xu, *React. Funct. Polym.* 66 (2006) 1272–1277.
- [21] W. Najjar, S. Azabou, S. Sayadi, A. Ghorbel, *Appl. Catal. B: Environ.* 88 (2009) 299–304.
- [22] A. Cuzzola, M. Bernini, P. Salvadori, *Appl. Catal. B: Environ.* 36 (2002) 231–237.
- [23] C.P. Huang, Y.H. Huang, *Appl. Catal. A: Gen.* 346 (2008) 140–148.
- [24] T.L.P. Dantas, V.P. Mendonc, H.J. Jose, *Chem. Eng. J.* 118 (2006) 77–82.
- [25] S. Li, H. Zhang, J. Wu, X. Ma, D. Yang, *Cryst. Growth Des.* 6 (2006) 351–353.
- [26] B. Tang, G. Wang, L. Zhuo, J. Ge, L. Cui, *Inorg. Chem.* 45 (2006) 5196–5200.
- [27] R. Matta, K. Hanna, S. Chiron, *Sci. Tot. Environ.* 385 (2007) 242–251.
- [28] F.C.C. Moura, M.H. Araujo, R.C.C. Costa, J.D. Fabris, J.D. Ardisson, W.A.A. Macedo, R.M. Lago, *Chemosphere* 60 (2005) 1118–1123.
- [29] R.C.C. Costa, M.F.F. Lelis, L.C.A. Oliveira, J.D. Fabris, J.D. Ardisson, R.R.V.A. Rios, C.N. Silva, R.M. Lago, *J. Hazard. Mater.* 129 (2006) 171–178.
- [30] C. Karunakaran, P. Anilkumar, *J. Mol. Catal. A: Chem.* 265 (2007) 153–158.
- [31] L.D. Kock, D. de Waal, *Spectrochim. Acta Part A* 71 (2008) 1348–1354.
- [32] I.V. Chernyshova, M.F. Hochella, A.S. Madden, *Phys. Chem. Chem. Phys.* 9 (2007) 1736–1750.
- [33] Y.Y. Xu, D. Zhao, X.J. Zhang, W.T. Jin, P. Kashkarov, H. Zhang, *Phys. E* 41 (2009) 806–811.
- [34] D. Bersani, P.P. Lottici, A. Montenero, *J. Raman Spectrosc.* 30 (1999) 355–360.
- [35] E.B. Hansson, M.S. Odziemkowski, R.W. Gillham, *Corros. Sci.* 48 (2006) 3767–3783.
- [36] A. Boughriet, B. Ouddane, C. Cordierc, J. Laureyns, *J. Chem. Soc. Faraday Trans.* 94 (1998) 3677–3683.
- [37] T. Yamamoto, T. Tanaka, S. Takenaka, S. Yoshida, *J. Phys. Chem. B* 103 (1999) 2385–2393.
- [38] F. Baillon, E. Provost, W. Fürst, *J. Mol. Liq.* 143 (2008) 8–12.
- [39] J. Baltrusaitis, D.M. Cwiertny, V.H. Grassian, *Phys. Chem. Chem. Phys.* 9 (2007) 5542–5554.
- [40] Y. Li, R.A. van Santen, Th. Weber, *J. Solid State Chem.* 181 (2008) 3151–3162.
- [41] W. Han, M. Gao, *Cryst. Growth Des.* 8 (2008) 1023–1030.
- [42] M. Descostes, F. Mercier, N. Thomat, C. Beaucaire, C. Beaucaire, M. Gautier-Soyer, *Appl. Surf. Sci.* 165 (2000) 288–302.
- [43] A.P. Grosvenor, B.A. Kobe, M.C. Biesinger, N.S. McIntyre, *Surf. Interf. Anal.* 36 (2004) 1564–1574.
- [44] W.M. Skinner, H.W. Nesbitt, A. Pratt, *Geochim. Cosmochim. Acta* 68 (2004) 2259–2263.
- [45] N. Gokulakrishnan, A. Pandurangan, P.K. Sinha, *Ind. Eng. Chem. Res.* 48 (2009) 1556–1561.
- [46] W. Freinbichler, K.F. Tipton, L.D. Corte, W. Linert, *J. Inorg. Biochem.* 103 (2009) 28–34.
- [47] X.W. Wu, D.J. Wu, X.J. Liu, *Appl. Phys. A* 97 (2009) 243–248.
- [48] Y. Cui, H. Du, L. Wen, *Solid State Commun.* 149 (2009) 634–637.
- [49] M. Hamadanian, A. Reisi-Vanani, A. Majedi, *Mater. Chem. Phys.* 116 (2009) 376–382.
- [50] D.B. Hamal, K.J. Klabunde, *J. Colloid Interf. Sci.* 311 (2007) 514–522.
- [51] X. Xue, K. Hanna, N. Deng, *J. Hazard. Mater.* 166 (2009) 407–414.
- [52] N.J. Cherepy, D.B. Liston, J.A. Lovejoy, H.M. Dong, J.Z. Zhang, *J. Phys. Chem. B* 102 (1998) 770–776.